Chapter 5
Hydrogen Embrittlement and "Cold Fusion" Effects in Palladium During Electrolysis Experiments

A. Carpinteri, O. Borla, A. Goi, S. Guastella, A. Manuello, and D. Veneziano

Abstract Recent experiments provided evidence of piezonuclear reactions occurring in condensed matter during fracture of solids, cavitation of liquids, and electrolysis. These experiments were characterized by significant neutron and alpha particle emissions, together with appreciable variations in the chemical composition. A mechanical reason for the so-called Cold Nuclear Fusion was recently proposed by the authors. The hydrogen embrittlement due to H atoms produced by the electrolysis plays an essential role for the observed microcracking in the electrode host metals (Pd, Ni, Fe, etc.). Consequently, our hypothesis is that piezonuclear fission reactions may occur in correspondence to the microcrack formation. In order to confirm the first results obtained by Co-Cr and Ni-Fe electrodes, electrolytic tests have been conducted using 100 % Pd at the cathode. As a result, relevant compositional changes and traces of elements previously absent have been observed on the Pd and Ni-Fe electrodes after the experiments and significant neutron emissions were observed during the test.

Keywords Hydrogen embrittlement • Cold fusion • Electrolysis • Piezonuclear reactions • Neutron emission

5.1 Introduction

Several evidences of anomalous nuclear reactions occurring in condensed matter were observed by different authors [1–34]. These experiments are characterized by extra heat generation, neutron emission, and alpha particle detection. Some of these studies, using electrolytic devices, reported also significant evidences of compositional variation after the microcraking of the electrodes [35–40].

In most of these experiments, the generated heat was calculated to be several times the input energy, and the neutron emission rate, during electrolysis, was measured to be about three times the natural background level [6]. In 1998, Mizuno presented the results of the measurements conducted by means of neutron detectors and compositional analysis techniques related to different electrolytic experiments. According to Preparata, "despite the great amount of experimental results observed by a large number of scientists, a unified interpretation and theory of these phenomena has not been accepted and their comprehension still remains unsolved" [6–9, 26, 27]. On the other hand, as shown by most of the articles devoted to Cold Nuclear Fusion, one of the principal features is the appearance of microcracks on electrode surfaces after the tests [26, 27]. Such evidence might be directly correlated to hydrogen embrittlement of the material composing the metal electrodes (Pd, Ni, Fe, Ti, etc.). This phenomenon, well-known in Metallurgy and Fracture Mechanics, characterizes metals during forming or finishing operations [41]. In the present study, the host metal matrix (Pd and Ni) is subjected to mechanical

A. Carpinteri (✉) • O. Borla • A. Manuello • D. Veneziano
Department of Structural, Geotechnical and Building Engineering, Politecnico di Torino, Corso Duca degli Abruzzi 24, 10129 Torino, Italy
e-mail: alberto.carpinteri@polito.it

A. Goi
Private Consultant

S. Guastella
Department of Applied Science and Technology, Geotechnical and Building Engineering, Politecnico di Torino, Corso Duca degli Abruzzi 24, 10129 Torino, Italy

N. Sottos et al. (eds.), *Experimental and Applied Mechanics, Volume 6: Proceedings of the 2014 Annual Conference on Experimental and Applied Mechanics*, Conference Proceedings of the Society for Experimental Mechanics Series,
DOI 10.1007/978-3-319-06989-0_5,

damaging and fracturing due to hydrogen atoms penetrating into the lattice structure and forcing it, during the gas loading. Hydrogen effects are largely studied especially in metal alloys where the hydrogen absorption is particularly high. The hydrogen atoms generate an internal stress that lowers the fracture resistance of the metal, so that brittle crack growth can occur with a hydrogen partial pressure below 1 atm [41, 42]. Some experimental evidence shows that neutron emissions may be strictly correlated to fracture of non-radioactive or inert materials. From this point of view, anomalous nuclear emissions and heat generation had been verified during fracture in fissile materials [2–4] and in deuterated solids [5, 8, 30]. The experiments recently carried out by Carpinteri et al. [36–39] represent the first evidence of neutron emissions from piezonuclear fissions occurring during the failure of inert, stable, and non-radioactive solids under compression, as well as from non-radioactive liquids under ultrasound cavitation [37, 38]. In the present paper, we analyze neutron and alpha particle emissions during tests conducted on an electrolytic cell, where the electrolysis is obtained using Ni-Fe and Pd electrodes in aqueous potassium carbonate solution. Voltage, current intensity, solution conductivity, temperature, alpha and neutron emissions were monitored. The compositions of the electrodes were analyzed both before and after the tests. Strong evidences suggest that the so-called Cold Nuclear Fusion, interpreted under the light of hydrogen embrittlement, may be explained by piezonuclear fission reactions occurring in the host metal, rather than by nuclear fusions of hydrogen isotopes adsorbed in the lattice. These results give an important confirmation about the hypothesis proposed by the authors and reported in previous papers on electrolysis with Ni-Fe and Cr-Co electrodes [43, 44].

5.2 Experimental Set Up

Over the last 10 years, specific experiments have been conducted on an electrolytic reactor (owners: Mr. A. Goi et al.). The aim was to investigate whether the anomalous heat generation may be correlated to a new type of nuclear reactions during electrolysis phenomena. The reactor was built in order to be appropriately filled with a salt solution of water and Potassium Carbonate (K_2CO_3). The electrolytic phenomenon was obtained using two metal electrodes immersed in the aqueous solution. The solution container, named also reaction chamber in the following, is a cylinder-shaped element of 100 mm diameter, 150 mm high, and 5 mm thick. For the reaction chamber Inox AISI 316 L steel was used. The two metallic electrodes were connected to a source of direct current: a Ni-Fe-based electrode as the positive pole (anode), and a Pd-based electrode as the negative pole (cathode).

The reaction chamber base consists of a ceramic plate preventing the direct contact between liquid solution and Teflon lid. Two threaded holes host the electrodes, which are screwed to the bottom of the chamber successively filled with the solution. A valve at the top of the cell allows the vapor to escape from the reactor and condense in an external collector. Externally, two circular Inox steel flanges, fastened by means of four threaded ties, hold the Teflon layers. The inferior steel flange of the reactor is connected to four supports isolated from the ground by means of rubber-based material. As mentioned before, a direct current passes through the anode and the cathode electrodes, provided by a power circuit connected to the power grid through an electric socket. The components of the circuit are an isolating transformer, an electronic variable transformer (Variac), and a diode bridge linked in series.

Electric current and voltage probes were positioned in different parts of the circuit. The voltage measurements were performed by a differential voltage probe of 100 MHz with a maximum rated voltage of 1,400 V. The current was measured by a Fluke I 310S probe with a maximum rated current of 30 A. Current intensity and voltage measurements were also taken by means of a multimeter positioned at the input line. From the turning on to the switching off of the electrolytic cell, current and voltage were found to vary in a range from 3 to 5 A and from 20 to 120 V, respectively.

For an accurate neutron emission evaluation, a He^3 proportional counter was employed (Xeram, France) with pre-amplification, amplification, and discrimination electronics directly connected to the detector tube. The detector is supplied by a high voltage power (about 1.3 kV) via NIM (Nuclear Instrument Module). The logic output producing the TTL (transistor–transistor logic) pulses is connected to a NIM counter. The logic output of the detector is enabled for analog signals exceeding 300 mV. This discrimination threshold is a consequence of the sensitivity of the He^3 detector to the gamma rays ensuing neutron emission in ordinary nuclear processes. This value has been determined by measuring the analog signal of the detector by means of a Co-60 gamma source. The detector is also calibrated at the factory for the measurement of thermal neutrons; its sensitivity is 65 cps/$n_{thermal}$ ($\pm$10 % declared by the factory), i.e., the flux of thermal neutrons is one thermal neutron/s cm^2, corresponding to a count rate of 65 cps. Finally, before and after the experiments, Energy Dispersive X-ray Spectroscopy has been performed in order to recognise possible direct evidence of piezonuclear reactions that can take place during the electrolysis. The elemental analyses were performed by a ZEISS Auriga field emission scanning electron microscope (FESEM) equipped with an Oxford INCA energy-dispersive X-ray detector (EDX) with a resolution of 124 eV @ MnKa. The energy used for the analyses was 18 KeV.

5.3 Neutron Emission Measurements

Neutron emission measurements performed during the experimental activity are represented in Fig. 5.1. The measurements performed by the He^3 detector were conducted for a total time of about 24 h. The background level was measured for different time intervals before and after switching on the reaction chamber. These measurements reported an average neutron background of about $(3.23 \pm 1.49) \times 10^{-2}$ cps. Furthermore, when the reaction chamber is active, it is possible to observe that, after a time interval of about 7.5 h (460 min), neutron emissions of about 3 times the background level may be detected. After 9 h (545 min) from the beginning of the measurements, it is possible to observe a neutron emission level of about one order of magnitude greater than the background level. Similar results were observed after 20 h (1,200 min) when neutron emissions up to 7 times the background were measured.

5.4 Compositional Analysis of the Pd Electrode

In the present section, the chemical compositions before and after the experiment will be taken into account, as well as the concentrations measured for each element identified on the surfaces of the two electrodes (see Tables 5.1 and 5.2).

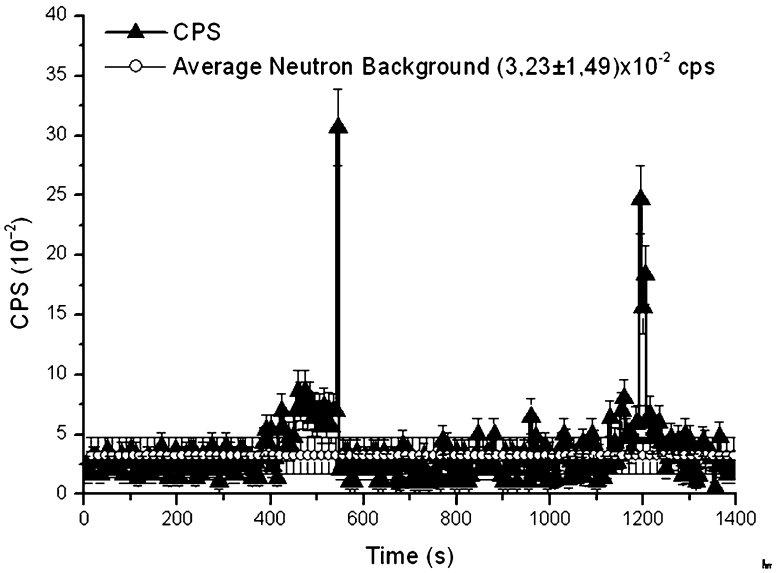

Fig. 5.1 Neutron emission measurements. Emissions between 3 times and 10 times the background level have been observed during the experiment

Table 5.1 Element concentrations before and after the electrolysis (Pd electrode)

	Average concentration		Average variation
Element	Before the experiment (%)	After 20 h (%)	(Negative for decrease) (%)
O	0.0	18.6	+18.5
Na	0.0	0.2	+0.2
Mg	0.0	1.0	+1.0
Al	0.0	0.4	+0.4
Si	0.0	1.1	+1.1
K	0.0	1.5	+1.5
Ca	0.0	0.2	+0.2
Cr	0.0	0.5	+0.5
Fe	0.0	2.0	+2.0
Co	0.0	0.2	+0.2
Cu	0.0	3.0	+3.0
Br	0.0	0.0	+0.0
Pd	100.0	71.3	−28.6

Table 5.2 Element concentrations before and after the electrolysis (Ni-Fe electrode)

	Average concentration		Average variation
Element	Before the experiment (%)	After 20 h (%)	(Negative for decrease) (%)
C	0.0	0.8	+0.8
O	2.0	21.5	+19.5
Al	0.0	1.8	+1.8
Si	0.3	1.1	+0.8
K	0.0	2.7	+2.7
Ti	3.4	3.0	−0.4
Cr	0.2	0.1	−0.2
Mn	0.0	0.1	+0.1
Fe	2.4	0.4	−2.0
Ni	91.6	68.5	−23.1

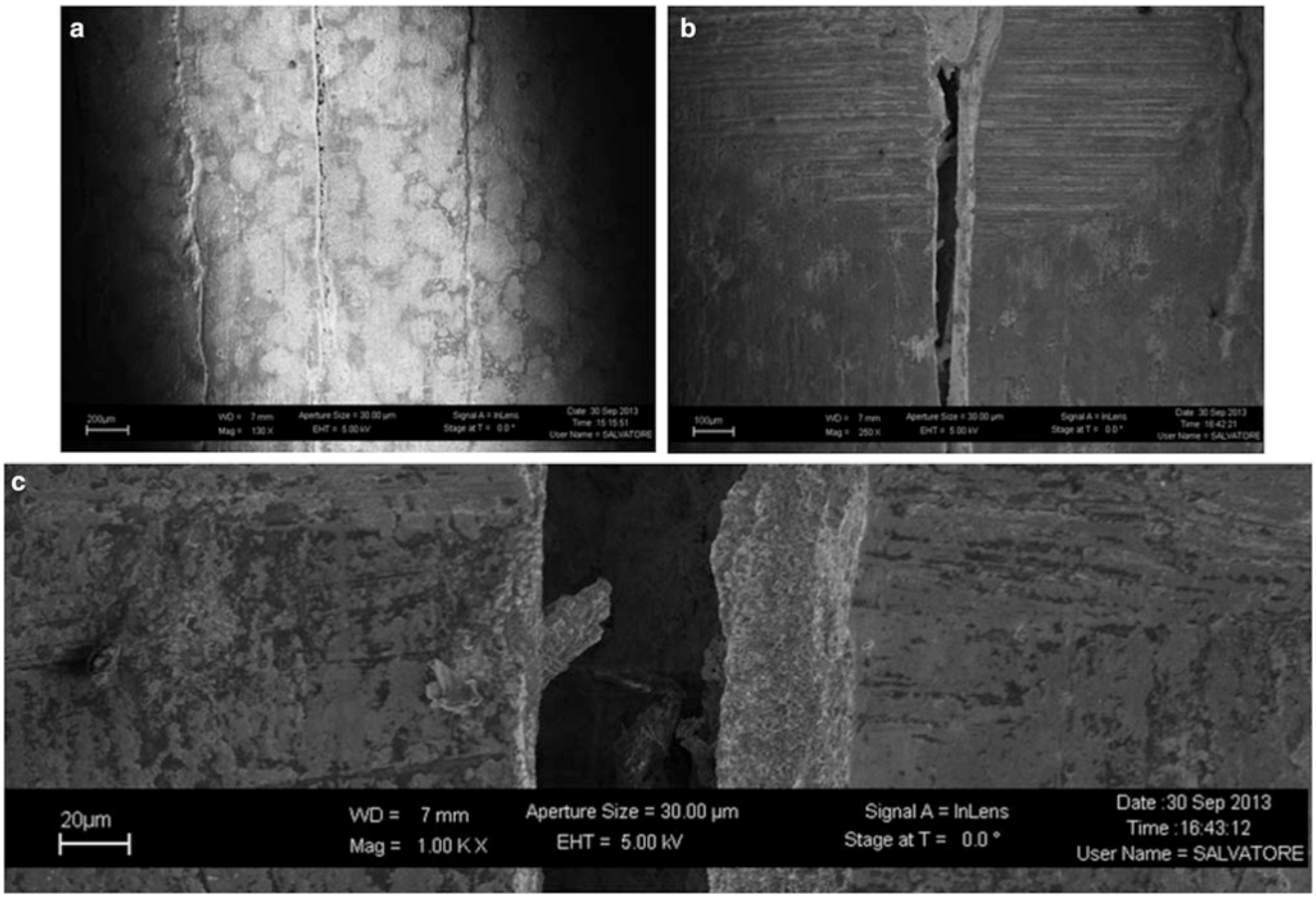

Fig. 5.2 Images (**a, b, c**) of the Palladium electrode surface: the fracture presented a width of about 40 µm and was observable at naked eyes

In particular, under the light of what can be deduced from the neutron emissions measurements and according to the hydrogen embrittlement hypothesis suggested by Carpinteri et al. [43, 44], the presence of microcracks and macrocracks on the electrode surface (Fig. 5.2a, b, c) is accounted in the mechanical interpretation of the phenomena. These evidences are particularly strong in the case of the Pd electrode, where a macroscopic fracture took place during the test. The fracture presented a width of about 40 µm observable at naked eyes (see Fig. 5.2c).

Considering the average decrement of Pd (−28.6 %), reported in Table 5.1, a first and fundamental fission reaction can be assumed:

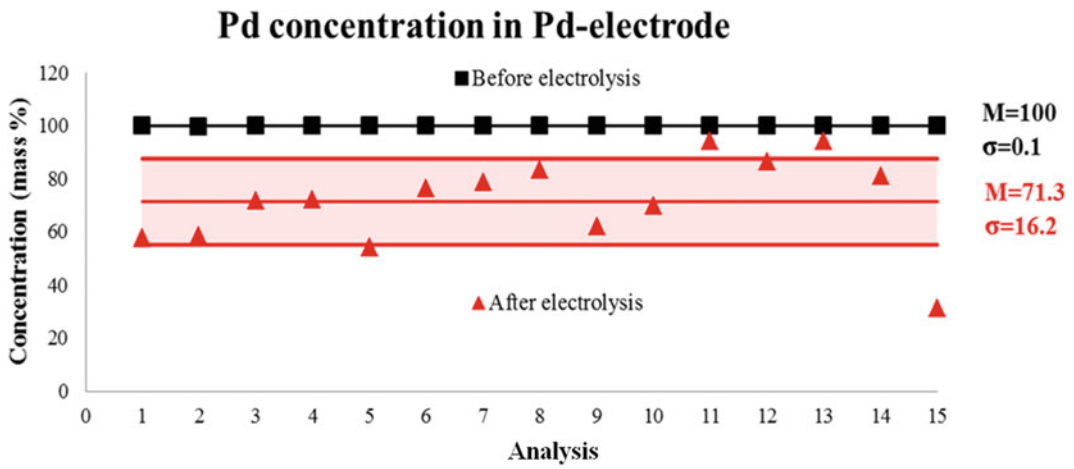

Fig. 5.3 Pd concentrations measured on 15 different points of the electrode surface, before (*square*) and after (*triangle*) the electrolysis; the average concentration M and the corresponding stand. dev. σ are reported

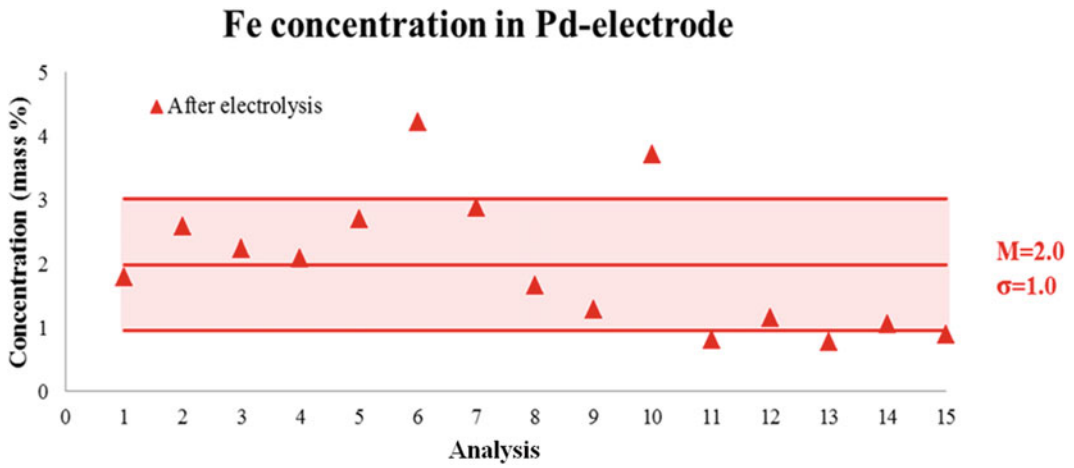

Fig. 5.4 Fe concentrations measured on the electrode surface after the electrolysis; Iron has not been detected before the experiment

$$\mathrm{Pd}_{46}^{106} \rightarrow \mathrm{Ca}_{20}^{40} + \mathrm{Fe}_{26}^{56} + 10 \ \text{neutrons} \tag{5.1}$$

According to reaction (5.1), the Pd decrement is counterbalanced by Ca and Fe increments by the following quantities: 10.8 and 15.1 %, for Ca and Fe, respectively. These variations may be accompanied by a neutron emissions corresponding to the remaining 2.7 % of the mass concentration (see also Figs. 5.3, 5.4, 5.5, and 5.6). The whole iron increment, according reaction (5.1), could be entirely considered as the starting element for the production of other elements. Hence, a second hypothesis can be proposed involving Fe as starting element and O as the product, together with alpha and neutron emissions:

$$\mathrm{Fe}_{26}^{56} \rightarrow 3\mathrm{O}_{8}^{16} + \mathrm{He}_{2}^{4} + 4 \ \text{neutrons} \tag{5.2}$$

According to reaction (5.2), the iron depletion produces 12.9 % of oxygen with alpha particles (He) and neutron emissions. The total measured increment in oxygen after the experimental test is equal to 18.5 % (see Table 5.1). This quantity seems to be only partially explained by reaction (5.2). The remaining 5.6 % of O concentration could be explained considering other reactions involving Ca (product in reaction 5.1) as the starting element:

$$\mathrm{Ca}_{20}^{40} \rightarrow \mathrm{O}_{8}^{16} + \mathrm{Mg}_{12}^{24} \tag{5.3}$$

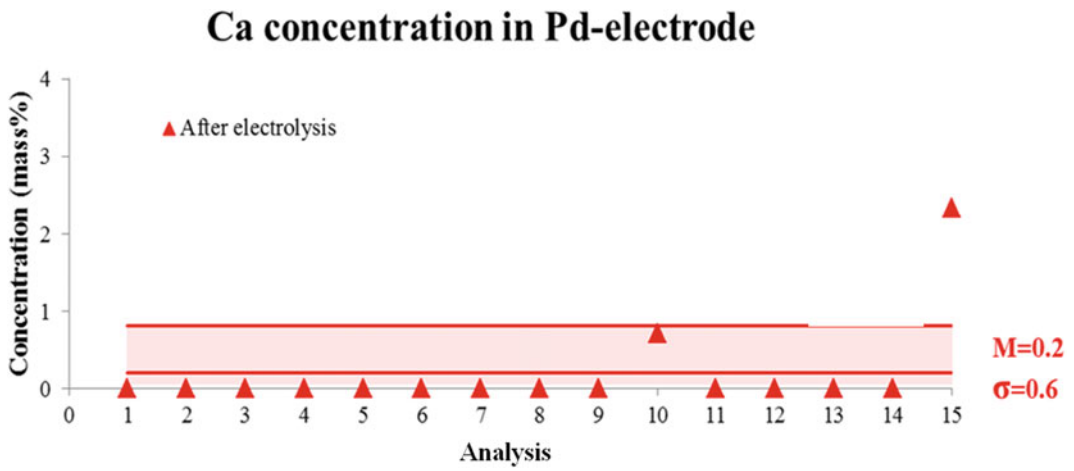

Fig. 5.5 Traces of Ca concentrations have been detected after the electrolysis

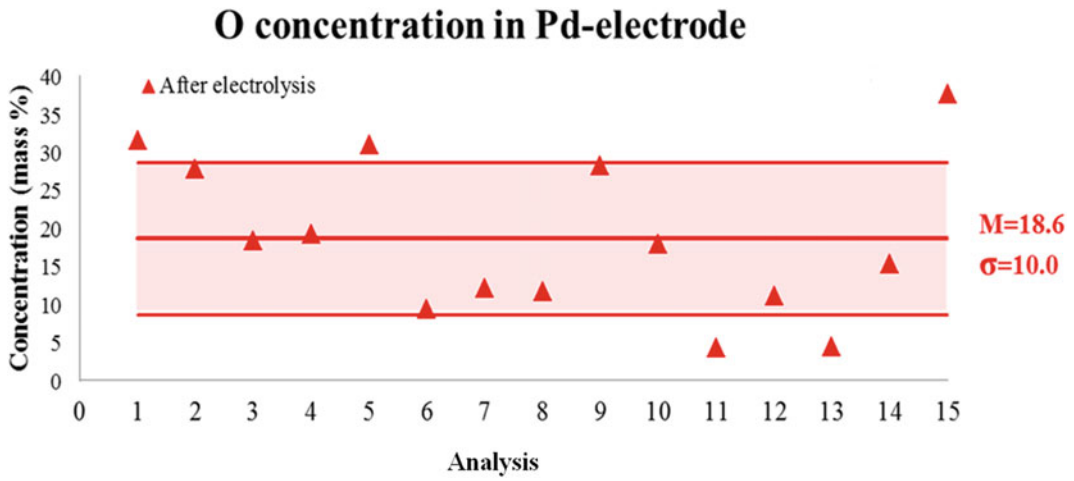

Fig. 5.6 The presence of the oxygen is remarkable after the experiments

$$\mathrm{Ca}_{20}^{40} \rightarrow 2\mathrm{O}_{8}^{16} + 4\mathrm{H}_{1}^{1} + 4 \text{ neutrons} \tag{5.4}$$

From reaction (5.3), we can consider a decrease in Ca concentration of 1.6 % and the formation of 1.0 % of Mg and 0.6 % of O. On the other hand, from reaction (5.4), we obtain a decrease in Ca equal to 5.9 %. This decrease gives an increase of 4.7 % in O and 0.6 in H, with neutron emissions equal to 0.6 %.

Considering the O increases coming from reactions (5.2), (5.3), and (5.4), totally equal to 18.2 %, and the experimental evidence reporting a total measured O concentration of 18.5 %, we may assume that O seems to be almost perfectly justified by the proposed reactions. At the same time, the Mg increment observed after the experiment can be explained by the results of reaction (5.3), see also Table 5.1. According to reactions (5.3) and (5.4), the following balances may be considered: Ca (−1.6 %) = Mg (+1.0 %) + O (+0.6 %); Ca (−5.9 %) = O (+4.7 %) + H (+0.6 %) + neutrons (+0.6 %). Taking into account the same reactions, and considering the Ca increase coming from reaction (5.1) (10.8 %), a concentration of 3.3 % of Ca remains to be counterbalanced. To this purpose, it is possible to take into account additional reactions involving Ca as starting element and Si, K and C as the results:

$$\mathrm{Ca}_{20}^{40} \rightarrow \mathrm{K}_{19}^{39} + \mathrm{H}_{1}^{1}, \tag{5.5}$$

$$\mathrm{Ca}_{20}^{40} \rightarrow \mathrm{C}_{6}^{12} + \mathrm{Si}_{14}^{28}. \tag{5.6}$$

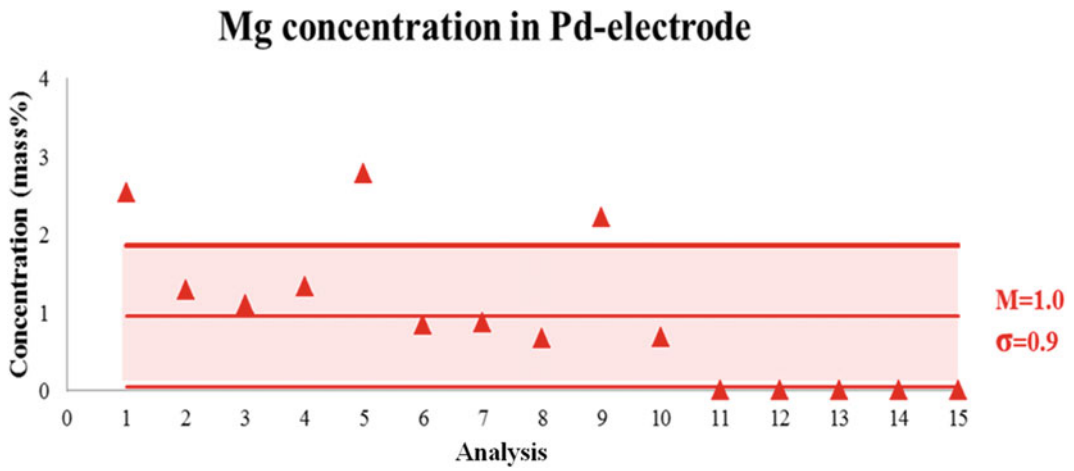

Fig. 5.7 The magnesium presence is evident after the experiment, while there was no trace of it before

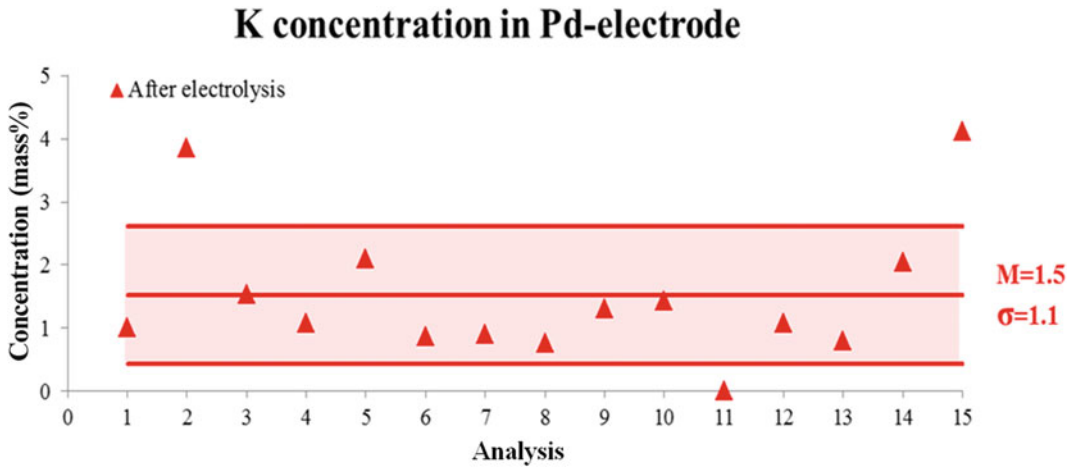

Fig. 5.8 Potassium evidences have been detected only after the experiment

From these reactions, the following balances may be considered: Ca (−1.6 %) = Si (+1.1 %) + C (+0.5 %); Ca (−1.5 %) = K (+1.5 %). Finally, considering the formation of 0.2 % of Ca after the experiment, the total Ca increase assumed by reaction (5.1) may be perfectly matched. The total Ca increment is equal to 10.8 %, the total Ca decrement by reactions (5.3), (5.4), (5.5), and (5.6) is 10.6 %, which returns a 0.2 % Ca concentration as measured. With regards to iron, its experimental compositional increase, measured on the Pd electrode, could be partially interpreted as an electrochemical effect due to the Fe decreasing in the Ni electrode. Finally, as for the final average variations in Mg (1.0 %), Si (1.1 %), and K (1.5 %), the hypotheses are perfectly consistent with the measured values (see Table 5.1 and Figs. 5.7, 5.8, and 5.9).

5.5 Nickel Electrode Composition Analysis

Let us consider the Nickel Electrode. Table 5.2 summarizes the concentration variations after the electrolysis. Nickel diminishes of 23.1 %, whereas the most apparent positive variation is that of oxygen (+19.5 %). It is worth noticing that the average concentration decrease in Fe (−2.0 %) is comparable to the average increase in Aluminum (+1.8 %). The Figs. 5.10, 5.11, 5.12, and 5.13 show the series of the concentrations measured before and after the experiment. In particular, when an element average concentration is zero, the corresponding series is absent: for instance, on the Ni electrode surfaces the Aluminum has not been detected before the electrolysis (Fig. 5.13).

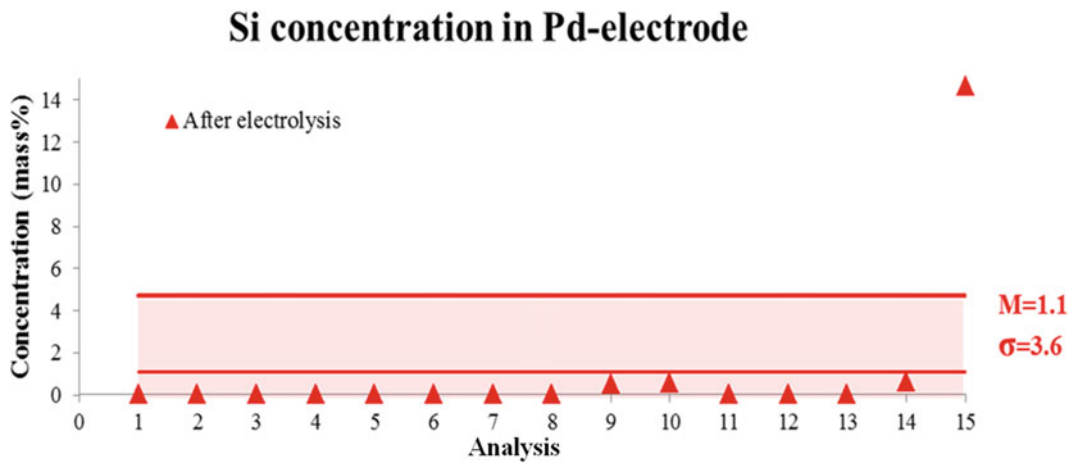

Fig. 5.9 EDS measures show evident traces of silicon only after electrolysis

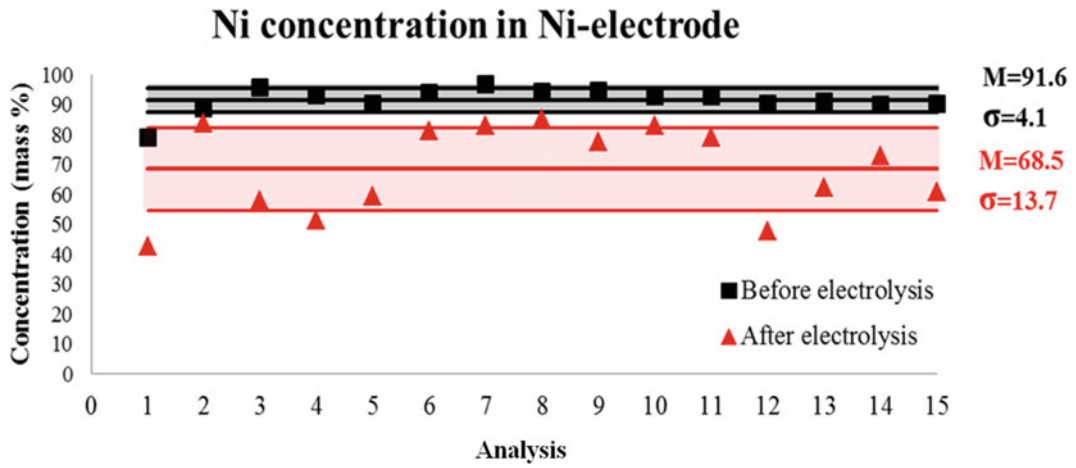

Fig. 5.10 Nickel electrode: the series of the Ni concentrations measured before and after 20 h of electrolysis are showed. An average variation between the two series of about 23.1 % may be considered

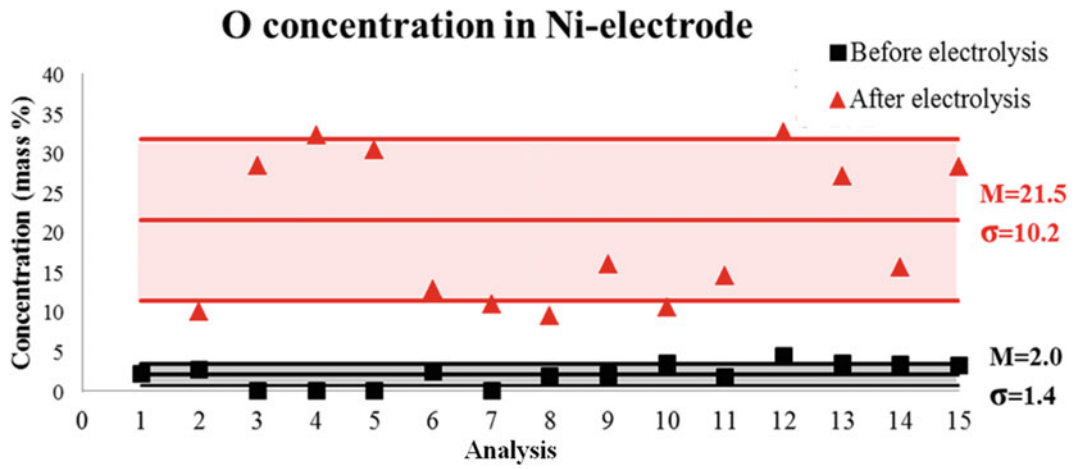

Fig. 5.11 O concentration before and after the experiment. The average values of O concentration change from a mass percentage of 2.0 % at the beginning of the experiment to 21.5 %

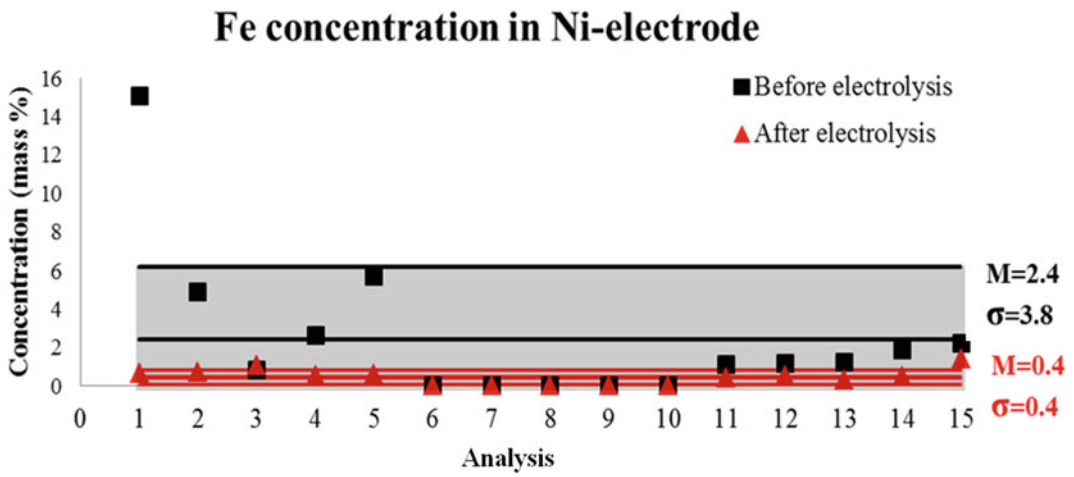

Fig. 5.12 Fe concentration before and after the experiment. The average values of Fe concentration change from a mass percentage of 0.4 % at the beginning of the experiment to 2.4 %

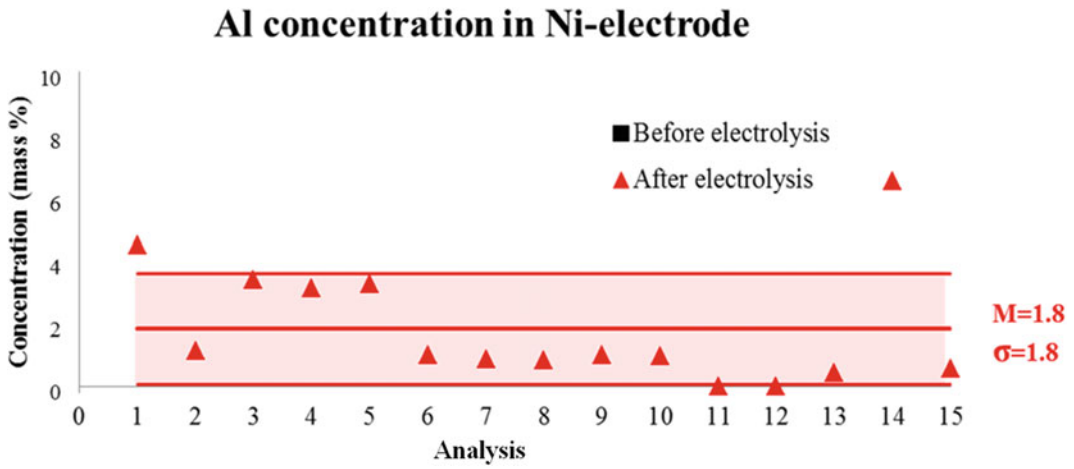

Fig. 5.13 Al concentration before and after the experiment. The average values of Al concentration (1.8 %) appear at the end of the test

On the basis of the piezonuclear reaction conjecture, we could assume the oxygen average variation as a nuclear effect caused by the following hypothesis:

$$\mathrm{Ni}_{28}^{59} \rightarrow 3\mathrm{O}_{8}^{16} + 2\mathrm{He}_{2}^{4} + 3 \text{ neutrons}. \tag{5.7}$$

A second hypothesis could be considered for the Al average variation, which could be consistent with the following:

$$\mathrm{Fe}_{26}^{56} \rightarrow 2\mathrm{Al}_{13}^{27} + 2 \text{ neutrons}. \tag{5.8}$$

A third hypothesis could be made considering the Silicon average variation:

$$\mathrm{Ni}_{28}^{59} \rightarrow 2\mathrm{Si}_{14}^{28} + 3 \text{ neutrons} \tag{5.9}$$

Reactions (5.7), (5.8), and (5.9) imply emissions of neutrons, which will provide a great support to the hypotheses based on piezonuclear reactions. The main idea underlying the hypothesis is that an average decrease of 23.1 % in Nickel underwent a reaction producing at least 18.8 % of oxygen together with alpha and neutron emissions. Secondly, an average depletion of 2 % in Fe would have produced about 1.8 % of Aluminum accompanied by neutron emissions. Thirdly, another average decrease in Ni of 1 % could have gone into Silicon (+0.9 %) and more neutrons. Considering the standard deviations

corresponding to each average concentration measured before and after the experiment (Figs. 5.10, 5.11, 5.12, and 5.13), the three considerations outlined above could be summarized according to the following balances: (1) Ni (−23.1 %) ≈ O (+18.8 %) + Si (+0.9 %) + alpha + neutrons, and (2) Fe (−2.0 %) ≈ Al (+1.8 %) + neutrons. Except for the Potassium increment (+2.7 %), which could be explained considering the deposition of the salt contained in the solution. The variations of the other elements' are lower than 1 %.

5.6 Conclusions

Neutron emissions up to one order of magnitude higher than the background level were observed during the operating time of an electrolytic cell. In particular, after a time span of about 7.5 h, neutron emissions of about 3 times the background level were measured. After 9 h and at the end of the test (after 20 h), it was possible to observe neutron emissions of about one order of magnitude greater than the background level.

By the EDX analysis performed on the two electrodes, significant compositional variations were recorded. In general, the decrements in Pd at the first electrode seem to be almost perfectly counterbalanced by the increments in lighter elements like oxygen. As far as the Ni-Fe electrode is concerned, the Ni decrement is almost perfectly counterbalanced by the O and Si increments according to reactions (5.7) and (5.9). At the same time, the Fe decrement may be considered to explain the final concentration of Al according to reaction (5.8). Chemical variations and energy emissions may be accounted for direct and indirect evidence of mechano-nuclear fission reactions correlated to microcrack formation and propagation due to hydrogen embrittlement. The so-called Cold Nuclear Fusion, interpreted under the light of hydrogen embrittlement, may be explained by piezonuclear fission reactions occurring in the host metal, rather than by nuclear fusion reactions of hydrogen isotopes forced into the metal lattice.

References

1. Borghi DC, Giori DC, Dall'Olio A (1992) Experimental evidence on the emission of neutrons from cold hydrogen plasma. In: Proceedings of the international workshop on few-body problems in low-energy physics, Alma-Ata, Kazakhstan, pp 147–154; Unpublished Communication (1957); Comunicacao n. 25 do CENUFPE, Recife Brazil (1971)
2. Diebner K (1962) Fusionsprozesse mit Hilfe konvergenter Stosswellen – einige aeltere und neuere Versuche und Ueberlegungen. Kerntechnik 3:89–93
3. Kaliski S (1978) Bi-conical system of concentric explosive compression of D-T. J Tech Phys 19:283–289
4. Winterberg F (1984) Autocatalytic fusion–fission implosions. Atomenergie-Kerntechnik 44:146
5. Derjaguin BV et al (1989) Titanium fracture yields neutrons? Nature 34:492
6. Fleischmann M, Pons S, Hawkins M (1989) Electrochemically induced nuclear fusion of deuterium. J Electroanal Chem 261:301
7. Bockris JO'M, Lin GH, Kainthla RC, Packham NJC, Velev O (1990) Does tritium form at electrodes by nuclear reactions? In: The first annual conference on cold fusion. National Cold Fusion Institute, University of Utah Research Park, Salt Lake City
8. Preparata G (1991) Some theories of cold fusion: a review. Fusion Technol 20:82
9. Preparata G (1991) A new look at solid-state fractures, particle emissions and "cold" nuclear fusion. Il Nuovo Cimento 104A:1259–1263
10. Mills RL, Kneizys P (1991) Excess heat production by the electrolysis of an aqueous potassium carbonate electrolyte and the implications for cold fusion. Fusion Technol 20:65
11. Notoya R, Enyo M (1992) Excess heat production during electrolysis of H_2O on Ni, Au, Ag and Sn electrodes in alkaline media. In: Proceedings of the third international conference on cold fusion, Nagoya, Japan. Universal Academy Press, Inc., Tokyo, Japan
12. Miles MH, Hollins RA, Bush BF, Lagowski JJ, Miles RE (1993) Correlation of excess power and helium production during D_2O and H_2O electrolysis using palladium cathodes. J Electroanal Chem vol 346:99–117
13. Bush RT, Eagleton RD (1993) Calorimetric studies for several light water electrolytic cells with nickel fibrex cathodes and electrolytes with alkali salts of potassium, rubidium, and cesium. In: Fourth international conference on cold fusion. Lahaina, Maui. Electric Power Research Institute, Palo Alto, CA
14. Fleischmann M, Pons S, Preparata G (1994) Possible theories of cold fusion. Nuovo Cimento Soc Ital Fis A 107:143
15. Szpak S, Mosier-Boss PA, Smith JJ (1994) Deuterium uptake during Pd-D codeposition. J Electroanal Chem 379:121
16. Sundaresan R, Bockris JOM (1994) Anomalous reactions during arcing between carbon rods in water. Fusion Technol 26:261
17. Arata Y, Zhang Y (1995) Achievement of solid-state plasma fusion ("cold-fusion"). Proc Jpn Acad 71(Ser. B):304–309
18. Ohmori T, Mizuno T, Enyo M (1996) Isotopic distributions of heavy metal elements produced during the light water electrolysis on gold electrodes. J New Energy 1(3):90
19. Monti RA (1996) Low energy nuclear reactions: experimental evidence for the alpha extended model of the atom. J New Energy 1(3):131
20. Monti RA (1998) Nuclear transmutation processes of lead, silver, thorium, uranium. In: The seventh international conference on cold fusion. ENECO Inc., Vancouver, Canada; Salt Lake City, UT

21. Ohmori T, Mizuno T (1998) Strong excess energy evolution, new element production, and electromagnetic wave and/or neutron emission in light water electrolysis with a tungsten cathode. Infinite Energy 20:14–17
22. Mizuno T (1998) Nuclear transmutation: the reality of cold fusion. Infinite Energy Press, Concord
23. Little SR, Puthoff HE, Little ME (1998) Search for excess heat from a Pt electrode discharge in K_2CO_3-H_2O and K_2CO_3-D_2O electrolytes
24. Ohmori T, Mizuno T (1999) Nuclear transmutation reaction caused by light water electrolysis on tungsten cathode under incandescent conditions. Infinite Energy 5(27):34
25. Ransford HE (1999) Non-stellar nucleosynthesis: transition metal production by DC plasma-discharge electrolysis using carbon electrodes in a non-metallic cell. Infinite Energy 4(23):16
26. Storms E (2000) Excess power production from platinum cathodes using the Pons-Fleischmann effect. In: 8th international conference on cold fusion. Lerici (La Spezia). Italian Physical Society, Bologna, Italy, pp 55–61
27. Storms E (2007) Science of low energy nuclear reaction: a comprehensive compilation of evidence and explanations about cold fusion. World Scientific, Singapore
28. Mizuno T et al (2000) Production of heat during plasma electrolysis. Jpn J Appl Phys A 39:6055
29. Warner J, Dash J, Frantz S (2002) Electrolysis of D2O with titanium cathodes: enhancement of excess heat and further evidence of possible transmutation. In: The ninth international conference on cold fusion. Tsinghua University, Beijing, China, p 404
30. Fujii MF et al (2002) Neutron emission from fracture of piezoelectric materials in deuterium atmosphere. Jpn J Appl Phys 41:2115–2119
31. Mosier-Boss PA et al (2007) Use of CR-39 in Pd/D co-deposition experiments. Eur Phys J Appl Phys 40:293–303
32. Swartz M (2008) Three physical regions of anomalous activity in deuterated palladium. Infinite Energy 14:19–31
33. Mosier-Boss PA et al (2010) Comparison of Pd/D co-deposition and DT neutron generated triple tracks observed in CR-39 detectors. Eur Phys J Appl Phys 51(2):20901–20911
34. Kanarev M, Mizuno T (2002) Cold fusion by plasma electrolysis of water. New Energy Technol 1:5–10
35. Cardone F, Mignani R (2004) Energy and geometry. World Scientific, Singapore, Chap. 10
36. Carpinteri A, Cardone F, Lacidogna G (2009) Piezonuclear neutrons from brittle fracture: early results of mechanical compression tests. Strain 45:332–339. (2009) Atti dell'Accademia delle Scienze di Torino 33:27–42
37. Cardone F, Carpinteri A, Lacidogna G (2009) Piezonuclear neutrons from fracturing of inert solids. Phys Lett A 373:4158–4163
38. Carpinteri A, Cardone F, Lacidogna G (2010) Energy emissions from failure phenomena: mechanical, electromagnetic, nuclear. Exp Mech 50:1235–1243
39. Carpinteri A, Lacidogna G, Manuello A, Borla O (2012) Piezonuclear fission reactions: evidences from microchemical analysis, neutron emission, and geological transformation. Rock Mech Rock Eng 45:445–459
40. Carpinteri A, Lacidogna G, Manuello A, Borla O (2013) Piezonuclear fission reactions from earthquakes and brittle rocks failure: evidence of neutron emission and nonradioactive product elements. Exp Mech 53:345–365
41. Milne I, Ritchie RO, Karihaloo B (2003) Comprehensive structural integrity: fracture of materials from nano to macro, vol 6. Elsevier, Amsterdam, pp 31–33, Chapter 6.02
42. Liebowitz H (1971) Fracture an advanced treatise. Academic, New York
43. Carpinteri A, Borla O, Goi A, Manuello A, Veneziano D (2013) Mechanical conjectures explaining cold nuclear fusion. In: Proceedings of the conference and exposition on experimental and applied mechanics (SEM), Lombard, Illinois, CD-ROM, Paper N. 481
44. Veneziano D, Borla O, Goi A, Manuello A, Carpinteri A (2013) Mechanical conjectures based on hydrogen embrittlement explaining cold nuclear fusion. In: Proceedings of the 21° congresso nazionale di meccanica teorica ed applicata (AIMETA), Torino, Italy, CD-ROM